Contents lists available at ScienceDirect

Nuclear Instruments and Methods in Physics Research A

Effects of beam-plasma instabilities on neutralized propagation of intense ion beams in background plasma ☆

Edward A. Startsev *, Igor D. Kaganovich, Ronald C. Davidson

Plasma Physics Laboratory, Princeton University, Princeton, New Jersey 08543, USA

ARTICLE INFO

ABSTRACT

The streaming of an intense ion beam relative to background plasma can cause the development of fast electrostatic collective instabilities. The plasma waves produced by the two-stream instability modify the ion beam current neutralization and produce non-linear average forces which can lead to defocusing of the ion beam. Recently, a theoretical model describing the average de-focusing forces acting on the beam ions has been developed, and the scalings of the forces with beam-plasma parameters have been identified (Startsev et al. in press[1]). These scalings can be used in the development of realistic ion beam compression scenarios in present and next-generation ion-beam-driven high energy density physics and heavy ion fusion experiments. In this paper the results of particle-in-cell simulations of ion beam propagation through neutralizing background plasma for NDCX-II parameters are presented. The simulation results show that the two-stream instability can play a significant role in the ion beam dynamics. The effects of velocity tilt on the development of the instability and ion beam compressibility for typical NDCX-II parameters are also simulated. It is shown that the two-stream instability may be an important factor in limiting the maximum longitudinal compression of the ion beam.

© 2013 Elsevier B.V. All rights reserved.

1. Introduction and theoretical model

In ion-beam-driven high energy density physics and heavy ion fusion applications, the intense ion beam pulse propagates through a background plasma before it is focused onto the target [1,2]. The streaming of the ion beam relative to the background plasma can cause the development of fast electrostatic collective instabilities [3]. These instabilities produces fluctuating electrostatic fields that cause a significant drag on the background plasma electrons and can accelerate electrons up to the average ion beam velocity. Consequently, the dominant electron current can reverse the beam self-magnetic field. As a result, the magnetic self-field force reverses sign and contributes to a transverse defocusing of the beam ions, instead of a pinching effect in the absence of instability [4,5]. In addition, the ponderomotive force of the unstable waves push background electrons transversely away from the resonant region inside the beam, which creates an ambipolar electric field, which also leads to ion beam transverse defocusing. Because the instability is resonant it is strongly affected and thus can be effectively mitigated and controlled by the longitudinal focusing of the ion beam [6–8].

Two-stream collective interactions between the beam ions and plasma electrons excite unstable waves with phase velocity ω/k_z slightly below the ion beam velocity v_b. Here ω is the unstable wave frequency and k_z is the unstable wave longitudinal wave-number (along the beam propagation direction z). In a recent publication [1] we have studied the nonlinear effects of a developed two-stream instability on a non-relativistic heavy ion beam with ions of mass m_b, charge $q=Z_b e$, density n_b, and longitudinal velocity $v_b \ll c$ during its propagation through cold neutralizing background plasma with density n_p and with no externally applied magnetic field. Here c is the speed of light. There, we developed a model that qualitatively captures the main nonlinear features that have been observed in numerical simulations of a proton beam propagating through a dense plasma background, and provides order-of-magnitude estimates of the average forces acting on the beam ions, provided that $Z_b n_b/n_p \ll 1$. Here we give a more complete elaboration of this model.

Due to the large beam ion mass $m_b \gg m_e$, where m_e is the electron mass, and for beams that are much longer than the resonant wavelength of the beam-plasma two-stream instability $l_b \gg v_b/\omega_{pe}$, where l_b is the beam length and $\omega_{pe}=(4\pi e^2 n_p/m_e)^{1/2}$ is the electron plasma frequency, the result of the instability is to produce short-wavelength electrostatic wave perturbations with frequency close to the plasma frequency $\omega \approx \omega_{pe}$. The unstable waves have a phase velocity which is close to the beam velocity, $\omega/k_z \approx \omega_p/k_z \approx v_b$. In what follows we assume that the beam transverse dimensions have a

single characteristic length of order of the beam radius r_b which is not much smaller than electron collisionless skin-depth, $r_b \gtrsim c/\omega_{pe}$. In this case $k_z r_b \gg 1$ and the instability is purely longitudinal. The radial dependence appears in all equations as a variable.

The unstable wave growth saturates either by longitudinal trapping of plasma electrons in the wave, which happens when the electron's amplitude of velocity oscillation in the wave become of order of the phase velocity of the wave $v_m^e \sim \omega/k_z \sim v_b$, or by trapping of beam ions, which happens when the beam ion's amplitude of velocity oscillation in the wave becomes of order of the difference between the beam velocity and the phase velocity of the wave $v_m^b \sim v_b - \omega/k_z \sim \gamma/k_z \approx (\gamma/\omega_{pe})v_b$. Here we used the fact that $\omega - k_z v_b \sim \gamma$, where $\gamma = \mathrm{Im}\,\omega \sim \omega_{pe}(\omega_{pb}/\omega_{pe})^{2/3}$ is the linear growth rate of the instability, and $\omega_{pb} = (4\pi Z_b^2 e^2 n_b/m_b)^{1/2}$ is the plasma frequency of the beam ions [9]. Because the electrons and beam ions both experience the same wave electric field, their oscillation velocities are related by $m_e \omega v_m^e = m_b(\omega - k_z v_b)v_m^b/Z_b$, or equivalently, $v_m^e \sim (m_b/Z_b m_e)(\gamma/\omega_{pe})v_m^b$. Therefore, if the beam ions become trapped by the wave before the electrons, $v_m^b \sim (\gamma/\omega_{pe})v_b$ and the corresponding amplitude of the electron velocity oscillations has to satisfy the relation $v_m^e \sim (m_b/Z_b m_e)(\gamma/\omega_{pe})^2 v_b \lesssim v_b$, or $[Z_b(m_b/m_e)(n_b/n_p)^2]^{1/3} \lesssim 1$. Otherwise, if $[Z_b(m_b/m_e)(n_b/n_p)^2]^{1/3} \gtrsim 1$, the electron velocity oscillation amplitude becomes $v_m^e \sim v_b$ first, and the saturation is determined by electron trapping. If the saturation is caused by beam ion trapping, the beam density becomes highly modulated in the longitudinal direction. The beam splits longitudinally into short bunches with length $\sim v_b/\omega_{pe} \ll l_b$.

The electric field of the waves also generates average transverse forces on the beam ions. An average ambipolar electric field is set up which acts against the Lorentz force and ponderomotive pressure of the wave exerted on the cold plasma electrons according to

$$e\langle E_x \rangle \sim e \frac{\langle v_z^e \rangle}{c}\langle B_y \rangle + m_e \frac{(v_m^e)^2}{4r_b}, \tag{1}$$

where r_b is the beam radius. At the same time, the wave electric field produces an average nonlinear electron longitudinal current density $\langle j_z^{non} \rangle = -e\langle \delta n^e \delta v_z^e \rangle \approx -e n_p \langle (\delta v_z^e)^2 \rangle/v_b \approx -e n_p (v_m^e)^2/2v_b$ in addition to the beam current density j_z^b. Here we used the linear relation $\delta n^e \approx n_p(k_z/\omega)\delta v_z^e \approx n_p \delta v_z^e/v_b$. The total injected current density $j_z^b + \langle j_z^{non} \rangle$ will produce an inductive plasma response current density $\langle j_z^{ind} \rangle = -e n_p \langle v_z^e \rangle$, which will reduce the total injected current density by the factor $1/(1 + r_b^2/\lambda_{pe}^2)$, where $\lambda_{pe} = c/\omega_{pe}$ is the collisionless skin-depth. Therefore the total current density in the plasma becomes
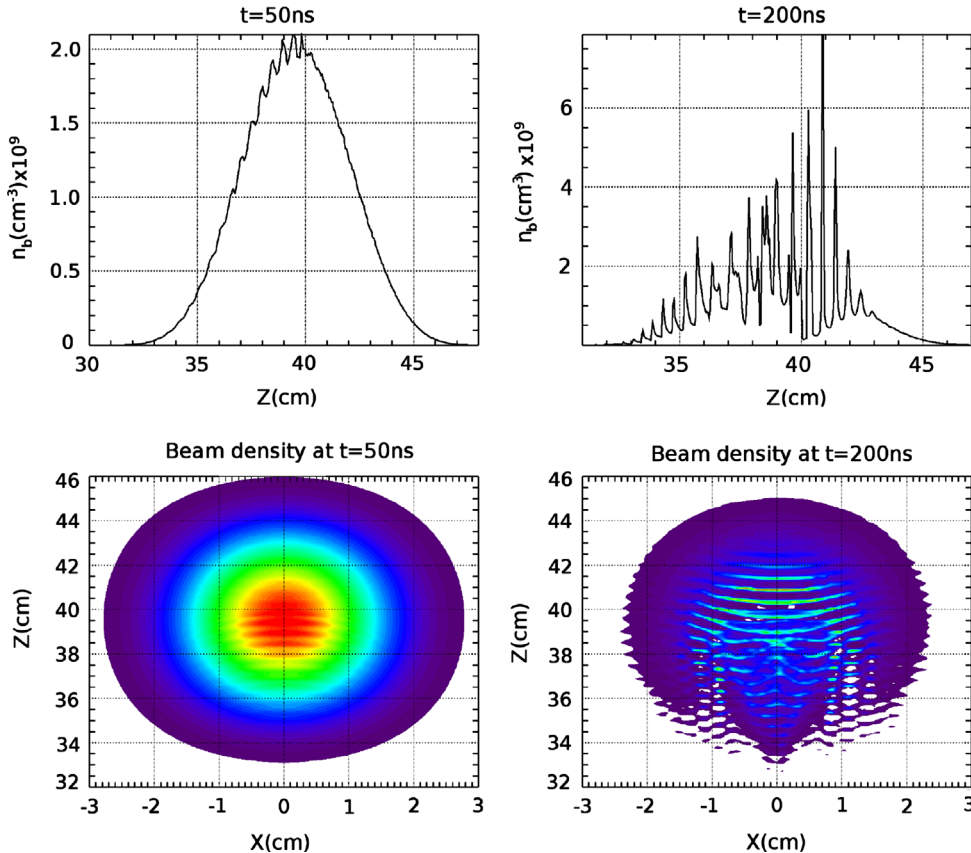
$$\langle j_z \rangle \approx \frac{j_z^b}{(1 + r_b^2/\lambda_{pe}^2)}\left[1 - \frac{1}{2}\frac{n_p}{Z_b n_b}\left(\frac{v_m^e}{v_b}\right)^2\right], \tag{2}$$

and the associated azimuthal self-magnetic field is

$$\langle B_y \rangle \sim \frac{2\pi}{c}\langle j_z \rangle r_b \sim \frac{2\pi Z_b e n_b r_b \beta_b}{(1 + r_b^2/\lambda_{pe}^2)}\left[1 - \frac{1}{2}\frac{n_p}{Z_b n_b}\left(\frac{v_m^e}{v_b}\right)^2\right]. \tag{3}$$

Note from Eqs. (2) and (3) that the presence of waves in the plasma due to the instability can cause the reversal of the total longitudinal current density and associated azimuthal self-magnetic field if $(v_m^e/v_b)^2 > (2Z_b n_b/n_p)$. The average electron flow produced by the inductive electric field ($\langle v_z^e \rangle \to 0$ as $c \to \infty$) is given by

$$\langle v_z^e \rangle \simeq \frac{Z_b n_b}{n_p}\frac{v_b}{(1 + \lambda_{pe}^2/r_b^2)}\left[1 - \frac{1}{2}\frac{n_p}{Z_b n_b}\left(\frac{v_m^e}{v_b}\right)^2\right]. \tag{4}$$

Fig. 1. Plots of ion beam density; beam density profile along $n_b(x=0, z, t)$ plotted versus z at $t = 50$ ns and $t = 200$ ns (top); beam density (x,z) contour plots at $t = 50$ ns and $t = 200$ ns (bottom).

The total average transverse force acting on the beam ions is given by

$$F_x = q\langle E_x \rangle - q\frac{v_b}{c}\langle B_y \rangle$$

$$\simeq Z_b e\frac{(\langle v_z^e \rangle - v_b)}{c}\langle B_y \rangle + m_e Z_b\frac{(v_m^e)^2}{4r_b}$$

$$\simeq m_e Z_b\left(\frac{v_b^2}{2r_b}\right)\left[\left(\frac{Z_b n_b}{n_p}\right) + x + \frac{x}{(1 + \lambda_{pe}^2/r_b^2)} + \frac{x^2}{(1 + \lambda_{pe}^2/r_b^2)^2}\right], \qquad (5)$$

where $x = (1/2)(v_m^e/v_b)^2 - Z_b n_b/n_p$.

The saturated level of the two-stream instability determines the magnitude of the average transverse force when $(1/2)(v_m^e/v_b)^2 \gg Z_b n_b/n_p$, or equivalently, the beam density is sufficiently large $(Z_b n_b/n_p)^{2/3} \gg (Z_b m_e/m_b)^{4/3}$. In that case $x > 0$, and the force is defocusing. For beams with $r_b \gg \lambda_{pe}$, the force on the beam ions is given by

$$F_x \simeq m_e Z_b\left(\frac{v_b^2}{2r_b}\right)[(x + 1)^2 - 1], \qquad (6)$$

where $x = (1/2)(v_m^e/v_b)^2$. For $(Z_b n_b/n_p)^{2/3} \gtrsim (Z_b m_e/m_b)^{1/3}$, the saturation is due to electron trapping, and $x \sim 1$ and $F_x \sim m_e Z_b v_b^2/r_b$, while for low-density beams with $(Z_b m_e/m_b)^{4/3} \ll (Z_b n_b/n_p)^{2/3} \lesssim (Z_b m_e/m_b)^{1/3}$, the saturation is by beam ion trapping and $x \sim (n_b/n_p)^{4/3}(Z_b m_b/m_e)^{2/3} \lesssim 1$, and the force is correspondingly smaller with $F_x \sim m_e Z_b v_b^2(n_b/n_p)^{4/3}(Z_b m_b/m_e)^{2/3}/r_b$. Given the transverse defocusing forces on the beam ions in Eq. (6), we can estimate the defocusing time $T \sim (m_b r_b/F_x)^{1/2}$ it takes the beam radius to double after the instability has developed and saturated, i.e., $\Delta r_b/r_b \simeq 1$ and the defocusing propagation distance is $L = v_b T$.

For sufficiently large beam density that $(Z_b n_b/n_p)^{2/3} \gtrsim (Z_b m_e/m_b)^{1/3}$, the defocusing time and distance are

$$T \sim \left(\frac{r_b}{v_b}\right)\left(\frac{m_b}{Z_b m_e}\right)^{1/2}, \quad L \sim r_b\left(\frac{m_b}{Z_b m_e}\right)^{1/2}, \qquad (7)$$

while for low density beams with $(Z_b m_e/m_b)^{4/3} \ll (Z_b n_b/n_p)^{2/3} \lesssim (Z_b m_e/m_b)^{1/3}$, the defocusing time and distance are

$$T \sim \left(\frac{r_b}{v_b}\right)\left(\frac{n_p}{Z_b n_b}\right)^{2/3}\left(\frac{m_b}{Z_b m_e}\right)^{1/6},$$

$$L \sim r_b\left(\frac{n_p}{Z_b n_b}\right)^{2/3}\left(\frac{m_b}{Z_b m_e}\right)^{1/6}. \qquad (8)$$

Note that the total defocusing time should also include the time for the instability to grow and saturate, $T_{sat} = (1/\gamma)\ln L$, where L depends on details of the beam density profile, and is a large number for sufficiently long, smooth beam profiles with $\omega_{pe}l_b/v_b \gg 1$.

2. Numerical simulations of NDCX-II experiment

In this section we present the results of numerical simulations using the particle-in-cell code LSP [10] of an intense ion beam propagating through neutralizing plasma with parameters relevant to the NDCX-II experiment [2]. The simulations were carried out in slab geometry $\partial/\partial y = 0$ with electric and magnetic field polarizations given by $\mathbf{E} = E_x\hat{\mathbf{e}}_x + E_z\hat{\mathbf{e}}_z$ and $\mathbf{B} = B_y\hat{\mathbf{e}}_y$. The simulations were carried out for the following parameters: a lithium ion beam with Gaussian density profile in both the longitudinal and
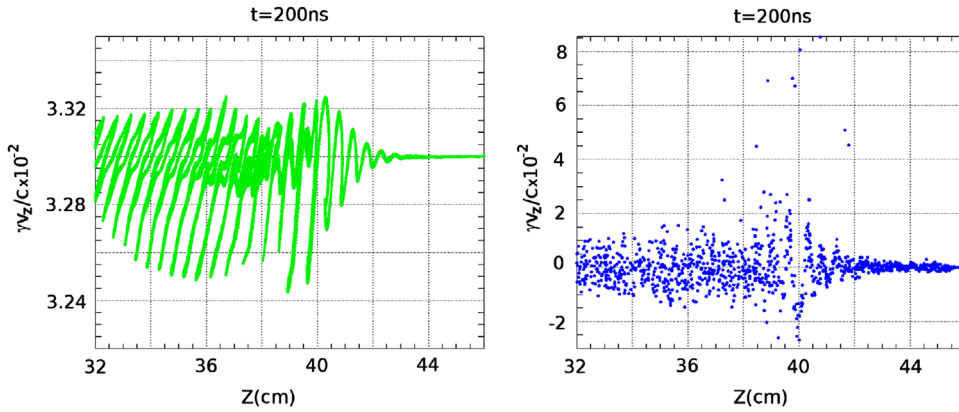
Fig. 2. Plots of beam ions (left) and plasma electrons (right) longitudinal phase-space $z-v_z\gamma/c$ at $t = 200$ ns.
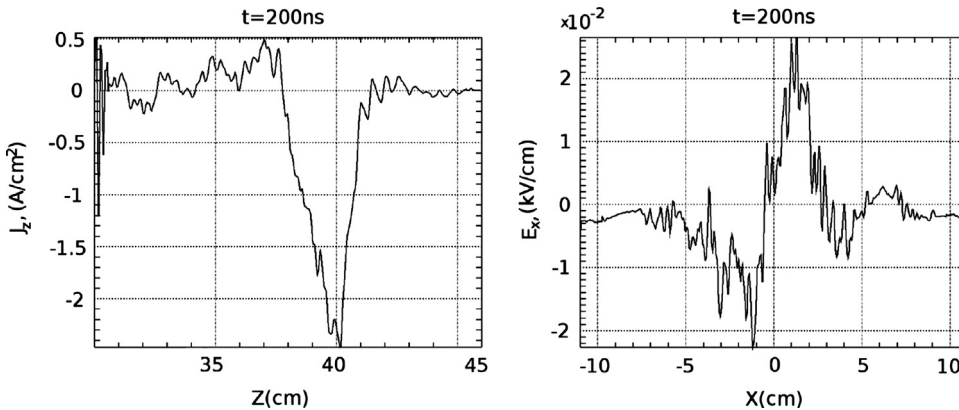
Fig. 3. Plots of total current density j_z at $r=0$ and transverse electric field E_x at $z=41$ cm at time $t = 200$ ns.
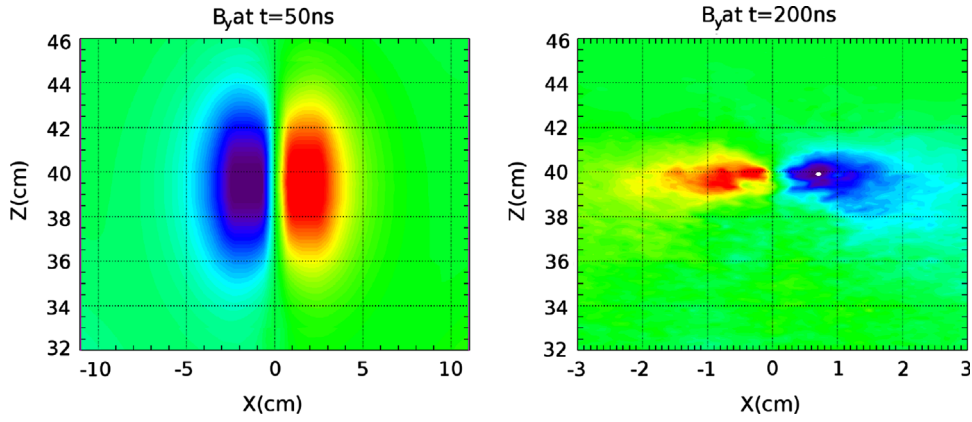
Fig. 4. Contour plots in (x,z) of self-magnetic field B_y at $t = 50$ ns and $t = 200$ ns.
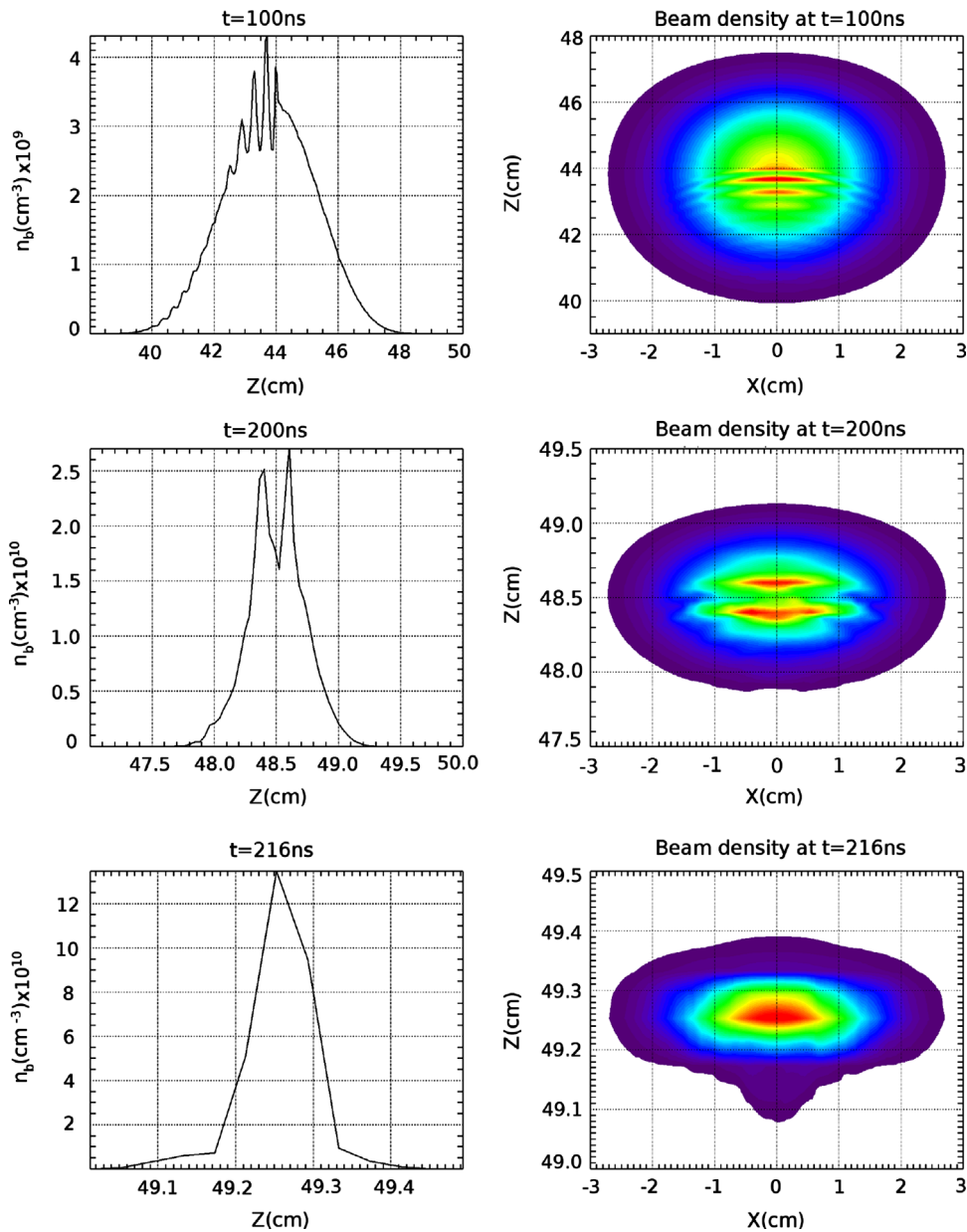

Fig. 5. Plots of ion beam density: beam density profile $n_b(x = 0, z, t)$ plotted versus z at $t = 100$ ns, $t = 200$ ns and $t = 216$ ns (left); beam density (x,z) contour plots at $t = 100$ ns, $t = 200$ ns and $t = 216$ ns (right).

transverse directions and pulse duration $T = 12$ ns. The beam velocity is $v_b = c/30$; the beam density is $n_b = 2 \times 10^9$ cm^{-3}; and the beam radius is $r_b = 1.41$ cm. The beam propagates through a stationary, singly-ionized carbon plasma with plasma density $n_p = 0.55 \times 10^{11}$ cm^{-3}. For these parameters, $r_b \sim \lambda_{pe} = c/\omega_{pe}$ and the characteristic linear exponentiation time of the two-stream instability is $\Gamma^{-1} = (\mathrm{Im}\,\omega)^{-1} = 4.1$ ns.

The results of the simulations are illustrated in Figs. 1–6. At time $t = 0$ the ion beam enters the plasma at $z = 0$. The changes in ion beam density profile during the beam propagation are shown in Fig. 1. At time $t = 50$ ns the two-stream instability between the beam ions and the plasma electrons begins to develop [Fig. 1(left)] and has completely developed to the saturation level by time $t = 200$ ns [Fig. 1(right)] (or two meters of propagation in the plasma). By this time, the beam density is modulated longitudinally with density variations of order 100% of the original beam density. This occurs because for the simulation parameters $[Z_b(m_b/m_e)(n_b/n_p)^2]^{1/3} \approx 2.6$ and therefore the trapping of both the beam ions and background electrons is responsible for saturation as shown in Fig. 2, where the longitudinal phase space $z - v_z\gamma/c$ is plotted for the beam ions and plasma electrons at $t = 200$ ns. Plots of the average total current density $<j_z>$ are shown in Fig. 3 at time $t = 200$ ns at the beam center $x = 0$, and plots of the transverse profile of average transverse electric field $<E_x>$ at $t = 200$ ns at the location of the maximum current density ($z = 41$ cm), which also correspond to the maximum amplitude of plasma oscillations.

The azimuthal magnetic field B_y is plotted in Fig. 4 at $t = 50$ ns (before saturation) and $t = 200$ ns (after saturation). Note that as the instability develops and saturates, the magnetic field changes sign because the current density $<j_z>$ becomes negative. Both the amplitude and the sign of the total current density and the amplitude and the sign of the ambipolar average transverse electric field are consistent with the theoretical estimates in Section 1. In the NDCX-II compression experiments, the beam enters the plasma with a velocity tilt $\Delta v_b/v_b = 0.1$, which should produce longitudinal beam compression after $t = 220$ ns. Note that even with zero velocity tilt, the two-stream instability leads to beam break-up at $t = 200$ ns, but no transverse defocusing Fig. 1. With velocity tilt $\Delta v_b/v_b = 0.1$, the instability does not develop enough to break-up the beam and prevent the longitudinal focusing.

Fig. 5 shows plots of the beam density profiles at different times during compression. A maximum longitudinal compression factor of $C = 67$ is achieved at $t = 216$ ns. Compression is limited by the instability spoiling the beam longitudinal phase space as shown in Fig. 6. The beam length at maximum compression corresponds to the size of the beam region where the initial linear velocity tilt was significantly spoiled by the instability, which (for this simulation) corresponds to one wavelength of the two-stream instability $\sim v_b/\omega_{pe}$ [Fig. 6]. Hence, the maximum compression was limited to $C \sim T\omega_{pe} \sim 100$.

3. Conclusions

The streaming of an intense ion beam relative to background plasma can cause the development of fast electrostatic collective instabilities. The present simulations of an intense ion beam
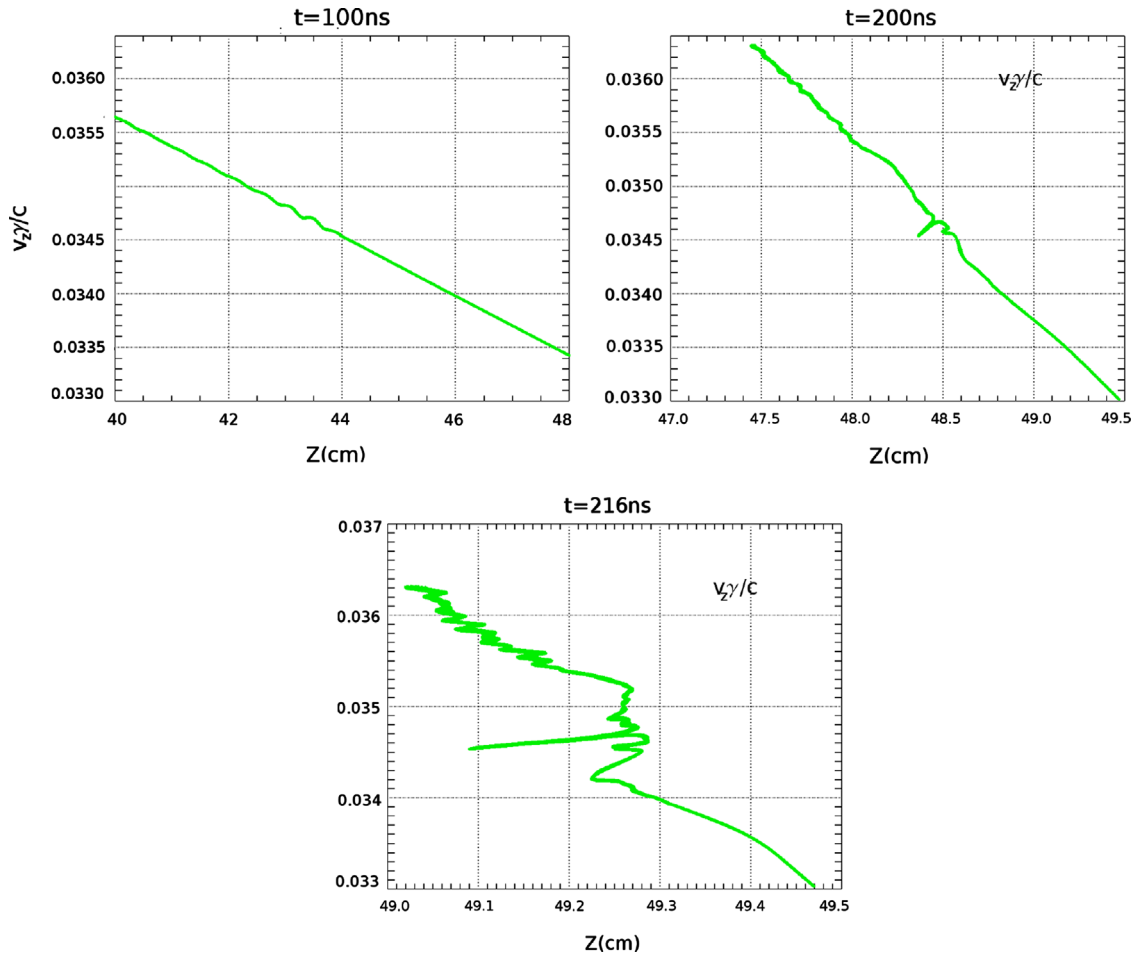

Fig. 6. Plots of beam ion longitudinal phase-space $z - v_z\gamma/c$ at $t = 100$ ns, $t = 200$ ns and $t = 216$ ns.

propagating though neutralizing plasma with parameters relevant to the NDCX-II experiment show that the instabilities produce fluctuating electrostatic fields that cause a significant drag on the background plasma electrons and can accelerate electrons up to velocities comparable to the ion beam velocity. Consequently, the (strong) electron current reverses the direction of the beam-induced self-magnetic field. As a result, the magnetic self-field force reverses sign and leads to a transverse defocusing of the beam ions, instead of a pinching effect in the absence of instability. In addition, the ponderomotive force [Eq. (1)] of the unstable waves pushes the background electrons transversely away from the unstable region inside the beam, which creates an ambipolar electric field, which also leads to a transverse defocusing of the beam ions [Eq. (5)]. The simple theoretical model that is presented in Section 1 provides order-of-magnitude estimates of the nonlinear defocusing forces that develop at saturation of the two-stream instability. In our simulations for beam parameters typical of NDCX-II, the nonlinear defocusing forces did not lead to any significant defocusing because of the short propagation distance of 2 m in background plasma, but they are expected to lead to a significant defocusing if the length of the neutralization section is increased by a sufficient amount.

Because the instability is resonant it is strongly affected and can be effectively mitigated and controlled by the longitudinal focusing of the ion beam. This is confirmed by simulations of an NDCX-II relevant beam compressing with velocity tilt $\Delta v_b / v_b = 0.1$. The two-stream instability gain for an ion beam with a velocity tilt which produces ion beam focusing in background plasma after time T_f is given by [6–8]

$$G = 0.8\omega_{pb}T_f, \tag{9}$$

where $\omega_{pb} \approx (4\pi e^2 n_b / m_b)^{1/2}$ is the ion beam plasma frequency. For NDCX-II parameters, $G \approx 4$ with $\exp(G) = 55$, and the initial density

perturbation grew due to instability large enough to spoil the liner velocity tilt only at the beam center, which prevented the beam from perfect longitudinal compression (Fig. 5). In contrast, the instability gain during the same time T_f for an NDCX-II beam with no velocity tilt is $G = \gamma T_f \approx 54$ with $\exp(G) = \exp(54)$ and the instability develops to the nonlinear saturation level well before time T_f and leads to longitudinal beam bunching (Fig. 1). Therefore, to avoid the effects of two-stream instability on the longitudinal beam compression, the beam density n_b or the beam compression time T_f have to be kept small enough to keep the instability gain for compressing beam small, $G = 0.8\omega_{pb}T_f \lesssim 1$.

References

[1] E.A. Startsev, I.D. Kaganovich, R.C. Davidson, European Physical Journal: Web of Conferences, 43, 2013, in press.
[2] A. Friedman, et al., Physics of Plasmas 17 (2010) 056704.
[3] R.C. Davidson, M. Dorf, I. Kaganovich, H. Qin, E.A. Startsev, S.M. Lund, Nuclear Instruments and Methods in Physics Research A 606 (2009) 11.
[4] I.D. Kaganovich, G. Shvets, E.A. Startsev, R.C. Davidson, Physics of Plasmas 8 (2001) 4180.
[5] R.N. Sudan, Physical Review Letters 37 (1976) 1613.
[6] E.A. Startsev, R.C. Davidson, M. Dorf, Nuclear Instruments and Methods in Physics Research A 606 (2009) 42.
[7] E.A. Startsev, R.C. Davidson, Nuclear Instruments and Methods in Physics Research A 577 (2007) 79.
[8] E.A. Startsev, R.C. Davidson, Physics of Plasmas 13 (2006) 062108.
[9] L.P. Pitaevskii, E.M. Lifshitz, Physical Kinetics (Course of Theoretical Physics), vol. 10, Butterworth-Heinemann, January 15, 1981.
[10] D.R. Welch, D.V. Rose, B.V. Oliver, R.E. Clark, Nuclear Instruments and Methods in Physics Research A 464 (2001) 134.